Coupled Systems Mechanics, *Vol. 7, No. 2 (2018) 233-254*
DOI: https://doi.org/10.12989/csm.2018.7.2.233

Long-term simulation of wind turbine structure for distributed loading describing long-term wind loads for preliminary design

Adnan Ibrahimbegovic* and Abir Boujelben

Sorbonne Universités, Université de Technologie Compiègne, Laboratoire Roberval de Mécanique, Chair of Computational Mechanics, Centre de Recherches Royallieu, CS 60319, 60200, Compiègne Cedex, France

(Received August 28, 2017, Revised September 27, 2017, Accepted September 28, 2017)

Abstract. In order to reduce the dependency on fossil fuels, a policy to increase the production capacity of wind turbine is set up. This can be achieved with increasing the dimensions of offshore wind turbine blades. However, this increase in size implies serious problems of stability and durability. Considering the cost of large turbines and financial consequences of their premature failure, it is imperative to carry out numerical simulations over long periods. Here, an energy-conserving time-stepping scheme is proposed in order to ensure the satisfying computation of long-term response. The proposed scheme is implemented for three-dimensional solid based on Biot strain measures, which is used for modeling flexible blades. The simulations are performed at full spatial scale. For reliable design process, the wind loads should be represented as realistically as possible, including the fluid-structure interaction (FSI) dynamic effects on wind turbine blades. However, full-scale 3D FSI simulations for long-term wind loading remain of prohibitive computation cost. Thus, the model to quantify the wind loads proposed here is a simple, but not too simple to be representative for preliminary design studies.

Keywords: wind turbine; wind load; energy-conserving scheme; long-term simulation

1. Introduction

Providing sufficient energy resources is an essential ingredient of socio-economic development and economic growth. According to statistics published by International-Energy-Agency, the global energy consumption for electricity has doubled since 1980's and this increase is expected to further accelerate in future. The crucial question is how to supply electricity without hazardous side effects of either CO_2 pollution with global warming typical of fossil fuel or radioactive waste storage problems of nuclear industry. The EU's energy and climate targets for 2030, in agreement with Europe's leading role in the fight against climate change, are at least 40% domestic reduction in greenhouse gas emissions compared to 1990 and at least 27% for the share of renewable energy consumed in the EU (EC 2017).

*Corresponding author, Professor, E-mail: adnan.ibrahimbegovic@utc.fr

http://www.techno-press.org/?journal=csm&subpage=8 ISSN: 2234-2184 (Print), 2234-2192 (Online)

The wind turbines that convert the energy contained in flowing air into electricity can be the right answer to producing clean and efficient energy and reducing the dependency on fossil fuels, if we manage to increase their production capacity (Hau 2006). This can be achieved with both increasing the size of wind turbines (Webb 2012) and placing them in offshore locations where the wind tends to blow harder and more uniformly than on land (Breton *et al.* 2009). This re-sizing is completely justified since the building and maintenance costs of wind turbine do not increase significantly with size. It is clearly more efficient opting for a single large wind turbine in hostile offshore location than wind turbine farms (see Fig. 1). The reason mainly lies with induced turbulence, so that each wind turbine will impact the efficiency and the proper operation of the others. In addition, the decrease in the number of wind turbines reduces the cost of foundation in the deep-sea and a considerable portion of the total cost pertaining to installation and maintenance.

Fig. 1(a) quest for design and construction of giant offshore wind turbine: Giant single wind turbine as opposed to wind turbine farms; (b) broken wind turbine blades and stability problem (C.C.K., Belgique Tournai - Bruges - région de Courtrai)

The EU has set an official challenge for building the prototype of a giant offshore wind turbine capable of producing more than 10 MW, requiring practically doubling the currently largest European installations. A quick estimate of the maximum wind turbine power P_{max}, [W] equal to 60% of kinetic energy of the air (with density ρ [kg/m^3]) passing with velocity V [m/s] through surface S [m^2] swept by the blades, ($P_{max} = {}^{16}/_{27} \times 0.5 \times \rho\, SV^3$) confirms that, for the average wind speeds of 10 m/s in the coastal European regions at 100 m altitude, this would require the turbine blades more than 100 m long. Thus, the first goal should be to ensure the integrity of the whole wind turbine in cases in which the blades will be designed as large as possible.

In shallow water areas typical of Denmark and Germany (see Fig. 2); the soil foundations are often used to install the wind turbine, so that the latter is anchored to the sea floor. However, if the water depth is more important, fixed foundations are no longer valid and floating supports are needed (Jonkman *et al.* 2011). That is the case, for instance, for the coastal western European regions (see Fig. 3). Thus, the second goal should be to ensure the stability of the floating sub-structure which, in turn, affects turbine blade design and wind turbine operating parameters.

Fig. 2(a) Offshore wind turbine foundations(Wikipedia, parc éolien de Thorntonbank); (b) Foundation fatigue testing (Germany); (c) floating offshore wind turbine, Semisubmersible column (WindFloat)

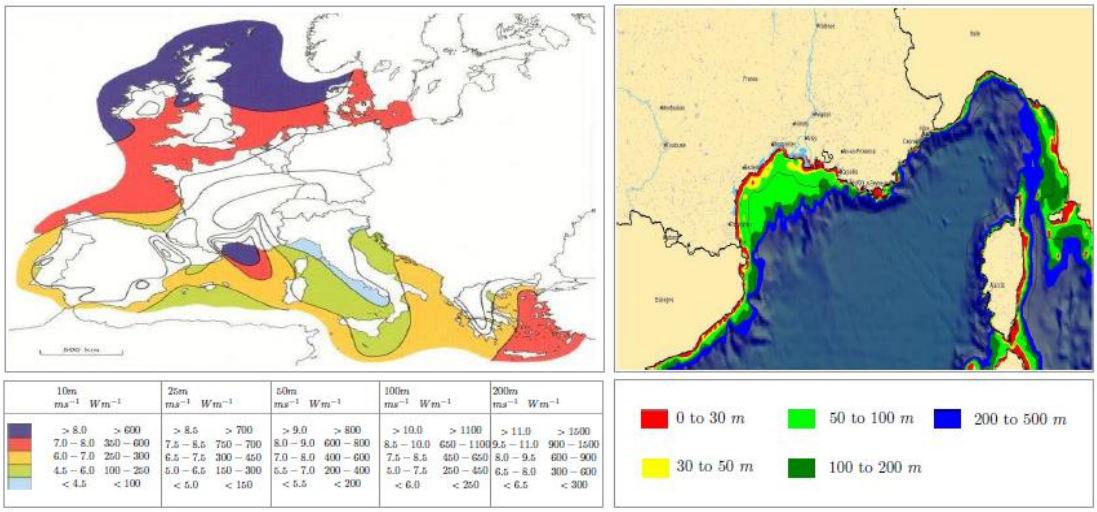

Fig. 3 Statistics on: (a) wind resources over open sea (more than 10 km offshore) for five different altitudes; (b) sea depth at different European coastal locations, showing marked difference between shallow water coast in Denmark and Germany versus deep water of Atlantic and Mediterranean coast (H. Boyé, l'éolien offshore)

The finite element approach is extremely efficient for structural dynamic analysis of wind turbine models. We have recently presented (Boujelben and Ibrahimbegovic 2017) full blades models using three-dimensional solid element with independent rotational degrees of freedom. The independent rotation field leads to the Biot strain measures. In view of the target size of the blades, they are assumed to be flexible and are subjected to large displacements and rotations during rotor operation. Thus, the finite element model of the blade deals with the theory of deformable solid body undergoing large motion.

Looking at an operating wind turbine, one may get the impression that the turbine turns

smoothly which corresponds to low frequency oscillations. However, literature results show that the motion of the wind turbine blade is also affected by high frequency oscillations caused mostly by the bending and torsional motion of the blade (Hansena *et al.* 2006). That implies a large difference between the high and low frequency modes leading to stiff problems. Since the standard implicit time-stepping schemes are not appropriate for analysis of such problems, we propose a development of robust time-stepping schemes capable of dealing with stiff problems. These schemes are needed to improve the numerical stability and in particular in long-term simulations.

Another important issue is the prediction of the loads on blades of the wind turbine. Clearly the loading regimes to which wind turbine can be subjected are extremely complex to analyze due to a variable set of environmental conditions. Particular attention is paid to aerodynamic loads derived from the force of the wind. There are well known approaches to calculate the aerodynamic loads: Blade Element Momentum method (BEM), Vortex method (VM) and Computational Fluid Dynamics (CFD). These different methods for accounting for dynamic analysis and fluid-structure interaction (FSI) effects will all have difficulties for long-term loading variations. Namely, each entails not only a high computational cost but also the complexity related to the definition of interface between fluid and structure domain. In order to reduce the complexities in view of design-oriented procedure, we propose an alternative method to determine aerodynamics load in terms of follower pressure loads. The latter can be directly applied to the wind turbine structural model replacing fluid-structure interaction.

The outline of the paper is as follows. In Section 2 we present a proposal for distributed loads applied to wind turbine blades for dynamic analysis. In Section 3 we examine in details the formulation and the numerical implementation of the proposed time-stepping energy conserving/decaying schemes for wind turbine structural model analysis. In Section 4 full-scale numerical simulations of a wind turbine model are presented in order to show the performance of the formulation proposed above. Some closing remarks are given in Section 5.

2. Proposal distributed loads: wind effects

Coupled fluid-structure interaction (FSI) simulations at full scale are particularly accurate for dynamic modeling of wind turbines. In fact, the motion and deformation of the wind turbine blades depend on the wind speed and vice versa. However, this approach increases significantly the complexity in terms of computational cost, convergence issues and interface representation between fluid and structure (Ibrahimbegovic *et al.* 2016). Although it has a high degree of accuracy, the fluid-structure interaction can only slow the computation process, which is undesirable in the first steps of preliminary design for wind turbine simulations. Here, we rather seek to develop a general model for follower pressure distributed on wind turbine blades with simplified approach to interaction. This model is suitable for dynamic time domain computations in order to facilitate the dynamic analysis of wind turbine structural models under long-term loading. We note in passing that detailed models of inelastic dynamic behavior (Do *et al.* 2015a, b, Imamovic *et al.* 2015) can be used subsequently for final comprehensive design.

Some important assumptions are used to develop this model:

i) Each blade does not impact the air for the following blade. The analysis of wind effects is limited to a single blade.

ii) The deformations of the blade do not have influence on the wind loading. In other words, the blade is considered as a rigid body only in the wind load modeling phase.

iii) The free stream velocity is considered constant over time (neglecting climate conditions), and it only depends on the height.

Based on the assumptions listed above, the aerodynamic load acting on the blade can be defined as a product of two functions: one time-dependent and another function of space. In the following, we explain how these functions are chosen in order to obtain the most reliable representation of the aerodynamic loads acting on the wind turbine blades.

2.1 Variation in time

Wind speed generally increases with height and this variation is referred to as wind shear. Sections of the wind turbine blades are exposed to airflow with different speeds according to its position. As shown in Fig. 4, two limiting cases are distinguished: the position (1) representing the position with the greatest wind speed and the position (2) where the speed is reduced to minimum. Since the distributed loading on the blades depends obviously upon the wind speed, it oscillates between two extremes with the periodic variations of this speed.

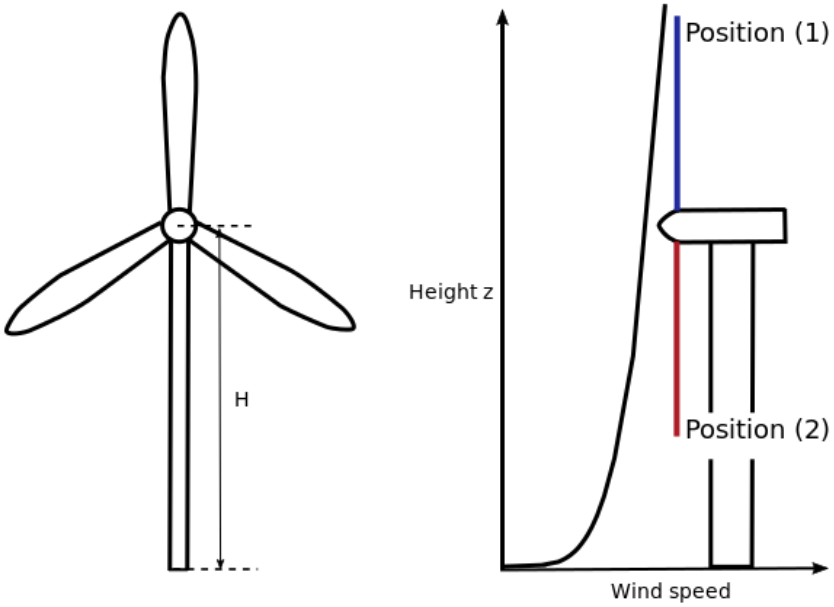

Fig. 4 Wind shear model: Variation of wind speed in height

When considering a single blade, during each rotation the distributed loading oscillates once because of the blade passing through minimum and maximum wind speeds in given wind shear. In view of these findings, we propose to introduce the variation in time through the following expression

$$\mathbf{f(t) = 1 + \varepsilon \cos(\omega t)} \tag{1}$$

Where ε is a parameter controlling the amplitude of pulsation whereas ω is chosen to be equal the rotation angular velocity of the blade. This expression concerns the blade that is initially

vertical. The time variation of others blades are obtained by introducing for each a shift phase angle in the cosine function. We note in passing that such an approach is suitable for fatigue failure studies under long-term variable loads cast within the framework of stochastic differential equations (Rocca *et al.* 2017).

The parameter is based on the model of wind speed variation. A common wind shear model is taken directly from the literature on wind turbine dynamics (Thresher *et al.* 1986). It is written as

$$\mathbf{V}(\mathbf{z}) = \mathbf{V_H}\left(\frac{\mathbf{z}}{\boldsymbol{H}}\right)^{\boldsymbol{\alpha}} \tag{2}$$

where $\mathbf{V_H}$ is the wind speed at top height, $\boldsymbol{\alpha}$ is the empirical wind shear exponent, $\boldsymbol{H}$ is the elevation of rotor housing, and $\mathbf{z}$ is the elevation above ground. In addition, the wind pressure is approximated by

$$\boldsymbol{P} = \frac{\mathbf{1}}{\mathbf{2}}\boldsymbol{\rho C_p V^2} \tag{3}$$

where $\boldsymbol{\rho}$ is the mass density of air and $\boldsymbol{C_p}$ is the pressure coefficient. From the relationship between pressures in the most favorable and unfavorable points, the parameter $\boldsymbol{\varepsilon}$ is defined by

$$\boldsymbol{\varepsilon} = \left[\left(\frac{\boldsymbol{H}+\boldsymbol{R}}{\boldsymbol{H}-\boldsymbol{R}}\right)^{2\boldsymbol{\alpha}} - \mathbf{1}\right] \Big/ \left[\left(\frac{\boldsymbol{H}+\boldsymbol{R}}{\boldsymbol{H}-\boldsymbol{R}}\right)^{2\boldsymbol{\alpha}} + \mathbf{1}\right] \tag{4}$$

where $\boldsymbol{R}$ is the radius of the rotor.

2.2 Variation in space

Concerning the variation in space, we consider classical aerodynamic modeling. There are several approaches to calculate the aerodynamic load. The latter depends mostly on the aerodynamic profiles of wind turbine blades and the angle of attack of the free stream. The approaches commonly used are: Blade Element Momentum (BEM) (Spera 1998), lifting line, panel and vortex methods (Katz *et al.* 1991, Cottet *et al.* 2000) and Computational Fluid Dynamics (CFD) (Sanderse *et al.* 2011, Lefrançois 2017).

The Blade Element Momentum offers a simple and fast way to simulate the aerodynamic forces on the blades. However, its accuracy depends upon the knowledge of the aerodynamic characteristics of the airfoil profile, obtained by wind tunnel testing. The latter needs high cost experimental equipments and a very specific knowledge for each new setting. Panel and vortex methods can offer a higher accuracy over the BEM method at the cost of a higher computational effort. They are useful to obtain a more detailed description of the 3D flow features around a wind turbine and their influence on the distributed loading on blades. Finally, full-scale Computational Fluid Dynamics tools (Ibrahimbegovic *et al.*2016) are very powerful, yet computationally very intensive to describe 3D flow features of the rotor. This is in general too costly to carry out full aerodynamic calculations for the case that concerns the parametric studies in preliminary design comparing several concepts.

In this paper, we therefore choose to use the 3D panel method instead. Such a choice remains sufficiently fast, yet reasonably accurate tool for preliminary design studies. The 3D panel method output can be cast in terms of distributed pressure loads representing the wind loads over each

panel, which can easily be transferred in the same format to the FE model used for structural dynamics computations. More specifically, the blade surface is divided into N panels, and 3D panel method provides the pressure in the center of each panel denoted by control point. We assume that the pressure is constant on each panel, and that it remains normal to the panel. It is thus represented by follower pressure loads applied on blades.

Some details pertaining to 3D panel method and follower pressure approach are given in this section.

2.2.1 Panel method

As previously mentioned, 3D panel method is discussed to solve aerodynamic steady state potential problems. The flow field around the blade is assumed to be incompressible $(\nabla . \mathbf{v} = 0)$ and in viscid ($\boldsymbol{\mu} = 0$). To obtain the solution by panel method, on one hand we require an impermeability condition on the surface and on the other hand accurate wake geometry to account for the downwash.

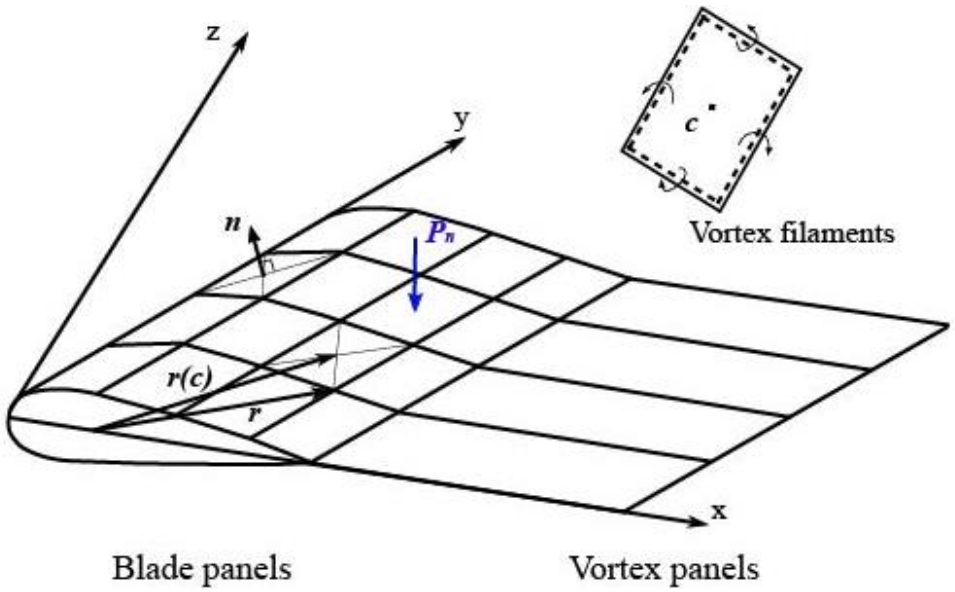

Fig. 5 Panel method mesh for wind turbine blade

As shown in Fig. 5, the blade's surface is divided in a number of panels. A closed vortex ring of constant strength $\boldsymbol{\Gamma}$ is placed on the panel. The wake is also modeled with a set of vortex rings behind the trailing edge of the blade. These vortex rings induce velocity components at the control point, designed by $\boldsymbol{V_d}$. The latter is given by the integral along the whole vortex ring

$$\boldsymbol{V_d} = \frac{\boldsymbol{\Gamma}}{\boldsymbol{4\Pi}} \int_c \frac{\boldsymbol{r}}{|\boldsymbol{r}|^3} \times \boldsymbol{dl} \tag{5}$$

where $\boldsymbol{r}$ is radial coordinate of the control point. Since the vortex rings are quadratic elements, the

easiest way to get $\boldsymbol{V_d}$ is to calculate the induced velocity of each vortex segment separately, resulting with

$$\boldsymbol{V_{d,1}} = \frac{\boldsymbol{\Gamma}}{\boldsymbol{4\Pi}} \frac{\boldsymbol{r_1 \times r_2}}{\left|\boldsymbol{r_1 \times r_2}\right|^2} \boldsymbol{r_c} . (\frac{\boldsymbol{r_1}}{\left|\boldsymbol{r_1}\right|} - \frac{\boldsymbol{r_2}}{\left|\boldsymbol{r_2}\right|}) \tag{6}$$

The impermeability condition is expressed by

$$\boldsymbol{V} . \boldsymbol{n} = \boldsymbol{0} \tag{7}$$

$\boldsymbol{V}$ represents the relative velocity, as the sum of the free stream velocity $\boldsymbol{V_\infty}$, the wind turbine blade rotation velocity component $\boldsymbol{V_r}$ $(\boldsymbol{V_r = \omega . r})$ and the interaction induced velocity $\boldsymbol{V_d}$. The vector $\boldsymbol{n}$ is the normal to the panel in the control point. The Eq. (7) becomes

$$(\boldsymbol{V_\infty + \omega . r + V_d}) . \boldsymbol{n} = \boldsymbol{0} \tag{8}$$

By substituting Eq. (5) into Eq. (8), we get a linear system of equation

$$\begin{bmatrix} \boldsymbol{a_{1,1}} & \boldsymbol{a_{1,2}} & \boldsymbol{\ldots} & \boldsymbol{a_{1,m}} \\ \boldsymbol{a_{2,1}} & \boldsymbol{a_{2,2}} & \boldsymbol{\ldots} & \boldsymbol{a_{2,m}} \\ \boldsymbol{.} & \boldsymbol{.} & \boldsymbol{.} & \boldsymbol{.} \\ \boldsymbol{.} & \boldsymbol{.} & \boldsymbol{.} & \boldsymbol{.} \\ \boldsymbol{a_{n,1}} & \boldsymbol{a_{n,2}} & \boldsymbol{\ldots} & \boldsymbol{a_{n,m}} \end{bmatrix} \begin{bmatrix} \boldsymbol{\Gamma_1} \\ \boldsymbol{\Gamma_2} \\ \boldsymbol{.} \\ \boldsymbol{.} \\ \boldsymbol{\Gamma_m} \end{bmatrix} = \begin{bmatrix} \boldsymbol{(V_\infty + \omega . r_1) . n_1} \\ \boldsymbol{(V_\infty + \omega . r_2) . n_2} \\ \boldsymbol{.} \\ \boldsymbol{.} \\ \boldsymbol{(V_\infty + \omega . r_n) . n_n} \end{bmatrix} \tag{9}$$

The last result shows that the normal induced velocities are written as a function of unknown strengths $\boldsymbol{\Gamma}_i$ and the influence coefficients $\boldsymbol{a}_{i,j}$. The influence coefficients correspond to the velocities due to the panels $\mathbf{m_i}$ at the control point of panel $\mathbf{n_j}$.

The system of Eq. (9) holds for the blade-on-blade interactions. We need to add the Kutta condition at the trailing edge to represent the influences of the wake on the blade.

$$\boldsymbol{\Gamma_{T.E}} = \boldsymbol{0} \tag{10}$$

This condition means that the wake panel strength $\boldsymbol{\Gamma_w}$ is equal to the strength of the difference between the last upper panel strength $\boldsymbol{\Gamma_u}$ and the last lower panel strength $\boldsymbol{\Gamma_l}$ (see Fig. 6), so that the flow would leave the trailing edge of a wing smoothly.

$$\boldsymbol{\Gamma_w} = \boldsymbol{\Gamma_u} - \boldsymbol{\Gamma_l} \tag{11}$$

By using the computed values of $\boldsymbol{\Gamma}$, the total velocity at each control point, defined in (8) is determined. We can then use Bernoulli to compute the coefficient of pressure for a panel $\mathbf{n}$

$$\boldsymbol{C_{pn}} = \boldsymbol{1} - \frac{\left|\boldsymbol{V_n}\right|^2}{\left|\boldsymbol{V_\infty}\right|^2} \tag{12}$$

Thus, the pressure $\boldsymbol{P_n}$ at each control point can be obtained directly as shown in (3). As already mentioned, this pressure is normal to the panel $\mathbf{n}$. Under the assumption that the pressure

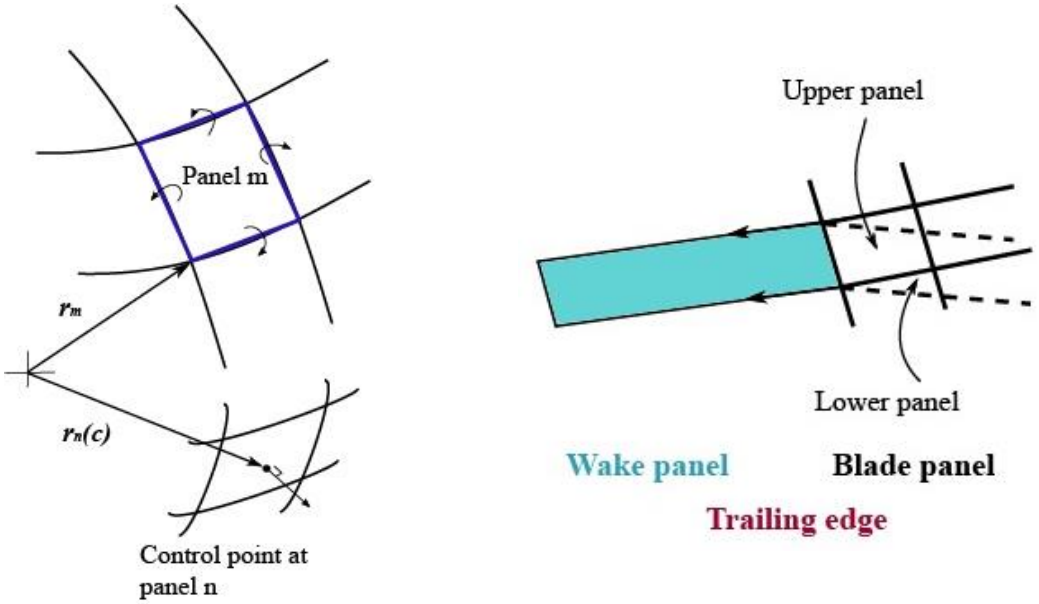

(a) Impermeability condition (b) Kutta condition

Fig. 6 Panel method conditions

distribution is uniform over a particular panel area, the total force on panel is written

$$\boldsymbol{F_n = \int_{S_p} P_n\, n\, dS} \tag{13}$$

2.2.2 Follower pressure approach

The panel method computation provides the value of pressure per panel. The pressure is applied in the direction of the normal in overall motion, i.e., the pressure direction follows the current configuration that is different from the initial configuration in large blade motion.

We consider $\boldsymbol{S_p}$ the panel surface where the pressure loading is applied. The corresponding surface in the deformed configuration is designed by $\boldsymbol{\varphi(S_p)}$ where $\boldsymbol{\varphi}$ is a point mapping, describing the evolution from the initial configuration to the deformations configuration. The weak form of the pressure boundary condition is written as

$$\boldsymbol{\bar{\Pi}(\varphi, \delta u) = \int_{\varphi(S_p)} P_n\, n\,.\,\delta u\, ds} \tag{14}$$

where $\boldsymbol{\delta u}$ is the virtual displacement vector.

The follower pressure approach relies on the parameterization of the moving surface $\boldsymbol{S_p}$ (Simo *et al.* 1991). This parameterization is constructed in two steps, as shown in Fig. 7. First, we carry out mapping from the isoparametric domain to the initial configuration, followed by the subsequent to the deformed configuration

$$\gamma := \varphi \circ \psi \tag{15}$$

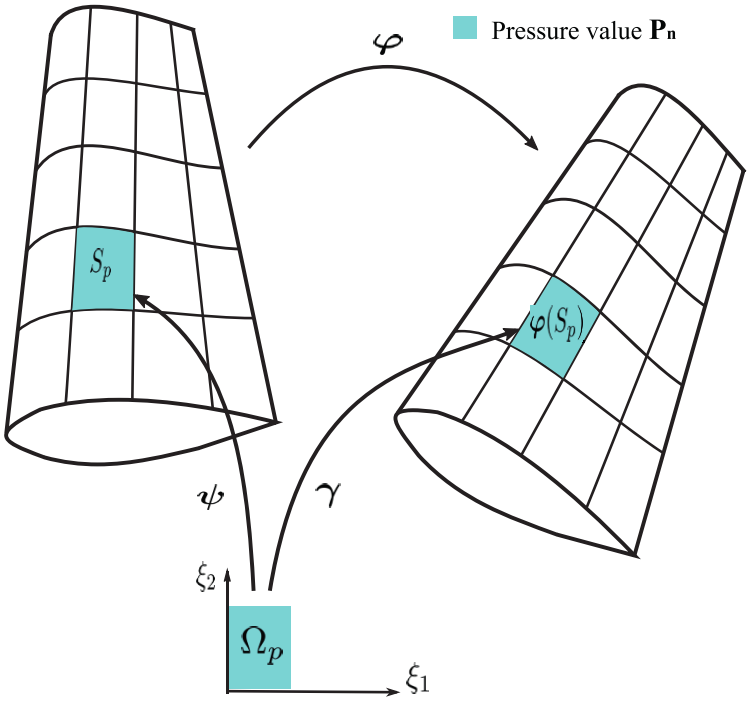

Fig. 7 Follower pressure loading: Parameterization of $\boldsymbol{\varphi(S_p)}$

The weak form defined in (14) becomes

$$\bar{\Pi}(\varphi, \delta u) = \int_{\Omega_p} P_n \left(\frac{\partial \gamma}{\partial \xi_1} \times \frac{\partial \gamma}{\partial \xi_2}\right) . \delta u \circ \gamma \; \partial \xi_1 \, \partial \xi_2 \tag{16}$$

For the finite element implementation, the blades are modeled with 8-nodes solid elements (Boujelben and Ibrahimbegovic 2017). The pressure loading will be associated with surface elements which are facets of these elements. Thus, the same mesh should be used for both panel method and FEM.

2.3 Final expression for applied load

At each panel of the blade surface, the pressure loading is finally written as

$$p(x,t) = f(t) * P_n(x) n(x) \tag{17}$$

The full FE model of wind turbine with three blades is constructed. The corresponding loads obtained from the formulas in (17) are transferred to the FE models for all blades. By taking into account the time variation, the proposal load model can provide the efficiency of structural

dynamics computations, especially for long-term loading pertinent to fatigue studies.

The proposed wind load approximation presents a quick and an efficient way to take into account the wind loading for dynamic wind turbines in preliminary design studies. These preliminary results can be taken as the basis for more detailed comprehensive studies by using full-scale fluid-structure interaction with high computational cost (Ibrahimbegovic *et al.* 2016).

3. Proposed time stepping scheme for long-term simulation

For structural analysis of the wind turbine, the finite element method (FEM) is used. The most FEM codes available today for wind turbine blade simulation, assume small deformations, which is not advisable when considering large overall motion of lengthy flexible blades (Ahlstrom 2006). The finite element model chosen herein is based upon the theory of deformable solid body submitted to large displacements, large rotations and large deformations (Ibrahimbegovic 2009).

More specifically, we choose 3D solid elements undergoing large motion for blade modeling (Boujelben and Ibrahimbegovic 2017). First, such elements can model the realistic shape of the blade without any a priori geometric simplification. Moreover, they allow retaining shape information on different regions of the blade much better than simplified beam models. The proposed 3D solid element includes both translation and rotation degrees of freedom that are introduced by the Biot strain measures (Biot 1965).

In this section, we present briefly the regularized variational formulation of the proposed 3D solid element with some details regarding conserving/decaying time stepping schemes. This type of schemes is of great interest for long-term simulations, which pertains to wind turbine modeling. Similar time stepping schemes have been developed for geometrically exact nonlinear beams (Ibrahimbegovic *et al.* 2002).

The equation of motion is obtained by appealing to the classical Hamilton principle employing the total energy functional, which consists of both potential and kinetic energy written as

$$H_D(u, \dot{u}, R) = T(\dot{u}) + \Pi(u, R, d) \tag{18}$$

where

$$\begin{aligned} T(\dot{u}) &= \int_V \frac{1}{2}\, \dot{u} \,.\, \rho \dot{u}\, dV \\ \Pi(u, R, d) &= \int_V \left\{ \frac{1}{2} sym[H].\, C\, sym[H] + \frac{1}{2} skew[H].\, \gamma\, skew[H] - P.\, d \right\} dV + \int_V u.\, f\, dV \end{aligned} \tag{19}$$

In (19) above, $\boldsymbol{H} = \boldsymbol{R}^T(\boldsymbol{I} + \boldsymbol{D}) - \boldsymbol{I}$ is the Biot strain measures, featuring large rotation tensor $\boldsymbol{R}$ obtained by polar decomposition of deformation gradient, $\boldsymbol{D}$ is the enhanced displacement gradient, given as a sum of the standard displacement gradient $\nabla \boldsymbol{u}$ and an enhanced displacement gradient $\boldsymbol{d}$ provided by the method of incompatible modes (Wilson *et al.* 1991). Finally, $\boldsymbol{P}$ is the first Piola-Kirchoff stress tensor whereas γ is the regularization parameter. An optimal value of γ , $\gamma = \mu$, is identified for both linear and nonlinear cases.

For computational efficiency, we further switch to the compact form of the matrix notation. The latter is presented in more detail in (Boujelben and Ibrahimbegovic 2017), Appendix (I). We denote with **N** and **L** the stress resultants, energy conjugate to the symmetric part and the skew-

symmetric part of the strain measures written in a matrix form as $\boldsymbol{e}$ and $\boldsymbol{\omega}$, respectively

$$N(u, R, d) := Ce(u, R, d); \quad L(u, R, d) := \gamma\omega(u, R, d) \tag{20}$$

The corresponding variational equations can be obtained by applying the variational principle

$$\begin{aligned}
&\begin{Bmatrix}\delta u\\ \delta w\end{Bmatrix}. r(u, R, d, p) := \int_V \delta\dot{u}.\, \rho\dot{u}\, dV + \int_V \left\{\delta e.\, N(u, R, d) + \delta\omega.\, L(u, R, d)\right\} dV - \int_V \delta u.\, f\, dV = 0\\
&\delta d.\, h(u, R, d, p) := \int_V \left\{\delta d.\, \Lambda^T(R) N(u, R, d) + \delta d.\, \Xi^T(R) L(u, R, d) - \delta d^T p\right\} dV = 0\\
&\delta p.\, g(u, R, d, p) := \int_V \left\{\delta p^T d\right\} dV = 0
\end{aligned} \tag{21}$$

The discrete approximation for the standard displacement field and rotation field are constructed according to the standard isoparametric interpolation for 8-nodes 3D solid element (Ibrahimbegovic 2009). The enhanced displacement gradient approximation is constructed by using derivatives of the incompatible displacements which are quadratic in order to improve the linear approximation of the 3D solid element (Wilson and Ibrahimbegovic 1991).

For computation at a typical time t_n, the values of u_n and R_n are known. The corresponding values at time t_{n+1} are computed in each step by using a single-step scheme. We use sample additive updates of displacement vector. However, the rotation tensor updates are somewhat more laborious by multiplicative type. With the aim of simplification, the rotation is defined by a quaternion representation, which reduces the rotation tensor to four parameters representation and provides a more efficient computational procedure for multiplicative rotation updates by replacing the matrix multiplication by the quaternion algebra (Spring 1986, Ibrahimbegovic 1997).

The proposed conserving/decaying time-stepping scheme is based on the midpoint approximation providing the time discretization of the weak form of the equations of motion

$$\begin{aligned}
&\int_V \delta u.\, \rho\ddot{u}_{n+\frac{1}{2}}\, dV + \int_V \left\{\delta e(u_{n+\frac{1}{2}}, R_{n+\frac{1}{2}}, d_{n+\frac{1}{2}}).\, N_{n+\frac{1}{2}} + \delta\omega(u_{n+\frac{1}{2}}, R_{n+\frac{1}{2}}, d_{n+\frac{1}{2}}).\, L_{n+\frac{1}{2}}\right\} dV\\
&- \int_V \delta u.\, f_{n+\frac{1}{2}}\, dV = 0\\
&\int_V \left\{\delta d.\, \Lambda^T(R_{n+\frac{1}{2}}) N_{n+\frac{1}{2}} + \delta d.\, \Xi^T(R_{n+\frac{1}{2}}) L_{n+\frac{1}{2}}\right\} dV = 0
\end{aligned} \tag{22}$$

where

$$\ddot{u}_{n+\frac{1}{2}} = \frac{\dot{u}_{n+1} - \dot{u}_n}{\Delta t}; \quad \dot{u}_{n+1} = -\dot{u}_n + \frac{2}{\Delta t} u_{n+1} \tag{23}$$

By using the approximation in (23), the first term in (22)1 can be written as the corresponding increment of kinetic energy

$$\Delta T = \int_V \delta u.\, \rho\ddot{u}_{n+\frac{1}{2}}\, dV = \int_V \frac{\Delta t}{2}(\dot{u}_{n+1} + \dot{u}_n).\, \rho\frac{1}{\Delta t}(\dot{u}_{n+1} - \dot{u}_n)\quad dV = T_{n+1} - T_n \tag{24}$$

To ensure that the rest of (22)1 gives the increment of internal energy, the stress resultants at $\boldsymbol{t}_{n+\frac{1}{2}}$ must be computed with algorithmic constitutive equations

$$N^{alg}_{n+\frac{1}{2}} = \frac{1}{2} C\,(e_{n+1} + e_n); \quad L^{alg}_{n+\frac{1}{2}} = \frac{1}{2}\gamma\,(\omega_{n+1} + \omega_n) \tag{25}$$

This leads to

$$\begin{aligned} \Delta\Pi_{\text{int}} &= \int_V \left\{ \delta e(u_{n+\frac{1}{2}}, R_{n+\frac{1}{2}}, d_{n+\frac{1}{2}}).\, N^{alg}_{n+\frac{1}{2}} + \delta\omega(u_{n+\frac{1}{2}}, R_{n+\frac{1}{2}}, d_{n+\frac{1}{2}}).\, L^{alg}_{n+\frac{1}{2}} \right\} dV \\ &= \int_V \left\{ \frac{1}{2}(e_{n+1} - e_n).\, C(e_{n+1} + e_n) + \frac{1}{2}(\omega_{n+1} - \omega_n).\, \gamma(\omega_{n+1} + \omega_n) \right\} dV \\ &= \Pi_{\text{int}}\big|_{n+1} - \Pi_{\text{int}}\big|_n \end{aligned} \tag{26}$$

Without loss of generality for applications, we assume that the external loading is obtained from a potential, which ensures $\Delta\Pi_{ext} = \Pi_{ext}\big|_{n+1} - \Pi_{ext}\big|_n$. Thus, with the results in (24) and (26), we get form (22)1

$$\begin{Bmatrix} \delta u \\ \delta w \end{Bmatrix}.\, r(u_{n+1}, R_{n+1}, d_{n+1}) = 0 \quad \longrightarrow \quad \underbrace{\Pi_{n+1}}_{\Pi_{ext}\big|_{n+1} + \Pi_{int}\big|_{n+1}} + T_{n+1} = \Pi_n + T_n \tag{27}$$

The proposed algorithmic is modified in order to control the effect of high frequency contribution, which can be difficult to solve mainly in the case of stiff problems. To that end, we add dissipation terms to the kinetic energy

$$\begin{aligned} u_{n+1} &= \frac{\Delta t}{2}\left[(\dot{u}_{n+1} + \dot{u}_n) + \eta_1 (\dot{u}_{n+1} - \dot{u}_n) \right] \\ \dot{u}_{n+1} &= \frac{1}{\Delta t(\frac{1}{2} + \eta_1)} u_{n+1} - \frac{\frac{1}{2} - \eta_1}{\frac{1}{2} + \eta_1} \dot{u}_n \end{aligned} \tag{28}$$

and also to the potential energy

$$N^{alg}_{n+\frac{1}{2}} = \frac{1}{2} C(e_{n+1} + e_n) + \eta_2\, C(e_{n+1} - e_n); \quad L^{alg}_{n+\frac{1}{2}} = \frac{1}{2}\gamma(\omega_{n+1} + \omega_n) + \eta_2\,\gamma(\omega_{n+1} - \omega_n) \tag{29}$$

where η_1 and η_2 are the dissipation coefficients, varying from **0** to **0.5**. By taking into account the velocity updates in (28), we can rewrite the kinetic energy increment (24)

$$\Delta T = \int_V \frac{1}{2}(\dot{u}_{n+1} + \dot{u}_n).\, \rho\,(\dot{u}_{n+1} - \dot{u}_n)\, dV + \eta_1 \int_V (\dot{u}_{n+1} - \dot{u}_n).\, \rho\,(\dot{u}_{n+1} - \dot{u}_n)\, dV = T_{n+1} - T_n + D_T \tag{30}$$

where $\boldsymbol{D}_T$ is the kinetic energy dissipation part. In addition, the corresponding evolution of

internal energy in (26) is rewritten

$$\begin{aligned}\Delta\Pi_{\text{int}} &= \int_V \left\{\frac{1}{2}(e_{n+1}-e_n).C(e_{n+1}+e_n)+\eta_2(e_{n+1}-e_n).C(e_{n+1}-e_n)\right\} \\ &+\left\{\frac{1}{2}(\omega_{n+1}-\omega_n).\gamma(\omega_{n+1}+\omega_n)+\eta_2(\omega_{n+1}-\omega_n).\gamma(\omega_{n+1}-\omega_n)\right\}dV \\ &= \int_V \frac{1}{2}\left\{(e_{n+1}-e_n).C(e_{n+1}+e_n)+(\omega_{n+1}-\omega_n).\gamma(\omega_{n+1}+\omega_n)\right\}\ dV \\ &+\int_V \eta_2\left\{(e_{n+1}-e_n).C(e_{n+1}-e_n)+(\omega_{n+1}-\omega_n).\gamma(\omega_{n+1}-\omega_n)\right\}dV \\ &= \Pi_{\text{int}}\big|_{n+1}-\Pi_{\text{int}}\big|_n+D_\Pi\end{aligned} \tag{31}$$

where D_Π presents the internal energy dissipation part. The energy dissipation parts having a positive definite quadratic form for positive values of η_1 and η_2, leading to

$$\begin{Bmatrix}\delta u\\ \delta w\end{Bmatrix}.r(u_{n+1},R_{n+1},d_{n+1})=0 \longrightarrow \underbrace{\Pi_{n+1}}_{\Pi_{ext}|_{n+1}+\Pi_{int}|_{n+1}}+T_{n+1}+D_\Pi+D_T \succ \Pi_n+T_n \tag{32}$$

It should be emphasized that the energy-decaying scheme is naturally constructed as an extension of the energy-conserving scheme with the introduction of the numerical dissipation in high modes at each step. In particular, the rotation update remains the same for both energy-conserving and energy-decaying schemes, which is quite useful for numerical implementation.

In general, the wind loads applied on the wind turbine blades are not conservative. Thus, the physical system does not conserve the total energy. However, by means of the proposed conserving time scheme, we can be sure that the variation of total energy does not appear from the spurious mode for large time steps, which ensures the robustness of the integration schemes. Hence, we will be able to run simulations over very long-time interval and avoid the undesirable instability effects in the case of stiff problems.

4. Numerical examples

As the first step, we construct a simple structural model of the wind turbine. As shown in Fig. 8, such a structural model is limited to the wind turbine blade, the housing, and their attachment zone. The tower can also be considered, if needed. The proposed model consists of three blades with a length of 63 meters. Each blade is composed mainly of the NACA64 profile (Law *et al.* 1987). Several airfoil types are provided in its first portion in order to ensure a smooth transition from the housing to the rotor and blade (see Fig. 9). The proposed 3D enhanced solid element is employed for modeling the FE model of the blade. The housing is represented by a revolute joint placed between two rigid bodies. The tower, which is 85 meters tall and with circular section, is modeled with geometrically exact beam undergoing large motion (Simo *et al.* 1986, Ibrahimbegovic 1995). All the computations are performed with a research version of the computer program FEAP, written by Prof. R.L. Taylor at UC Berkeley (Zienkiewicz *et al.* 1989).

4.1 Validation of the proposal wind pressure

For the proposed blade model, the aerodynamic surface is divided into $\boldsymbol{N = nb \times ns}$ panels where $\boldsymbol{nb}$ is the number of nodes in the span direction and $\boldsymbol{ns}$ is the number of nodes of the aerodynamic profile approximation. The distributed pressure is computed by means of panel method as shown in Section 2. The parameter ε is computed with the formula (4) by taking the empirical wind shear exponent $\boldsymbol{\alpha}$ equal to 0.13. This value corresponds to open water cases e.g., offshore wind turbines (Hsu *et al.* 1994).

The total force per span-wise section is calculated in order to investigate how the aerodynamic force varies along the blade span. The wind speed is uniform at 10 m/s and the rotor speed is imposed equal to 12.1 *rpm*. The chosen values correspond to one of the cases given in (Jonkman *et al.* 2005), where the aerodynamics simulations are performed for 5-MW reference wind turbine placed in offshore location.

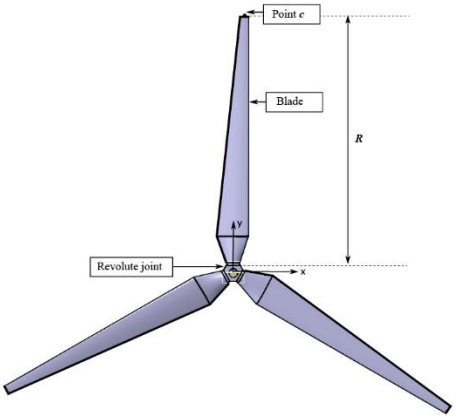

Fig. 8 Geometric model of the wind turbine

The variation of the aerodynamic force as function of blade span is given in Fig. 10, for different mesh configurations. The obtained curves are in good correspondence with the results in (Bazilevs *et al.* 2012) obtained by full-size FSI model. Mesh refinement study indicates good convergence in wind load representation. Moreover, since the same mesh is used for panel method for fluid and FEM for blades, it is ensured that no specific mesh requirements are imposed by panel method.

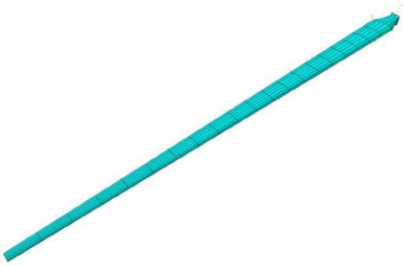

Fig. 9 Example of FE mesh for blade, with the same mesh used for Panel method for fluid

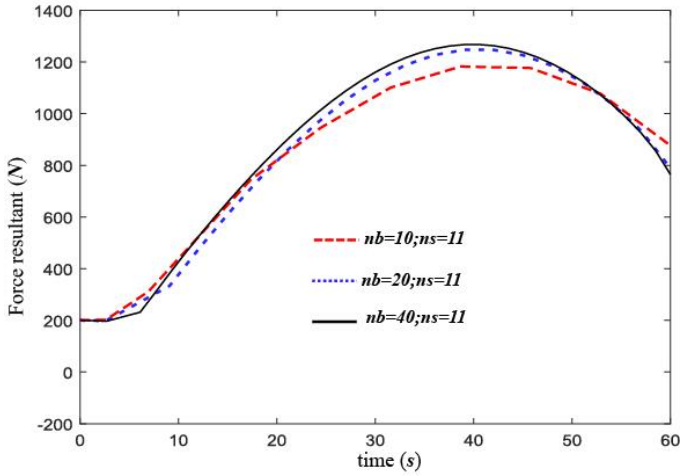

Fig. 10 Panel method: Aerodynamic force as function of blade span

The wind turbine model without tower is considered. The shaft is clamped. For each blade, the selected value of Young's modulus is $\boldsymbol{E}$ = 2754.6 *MPa* and Poisson's ratio is $\boldsymbol{\nu}$ = 0. The mass density is chosen as $\boldsymbol{\rho}$ = 1.85 g/cm^3. These values are corresponding to glass reinforced epoxy resin material (Siemens AG 2011). For the operating conditions selected above, the distributed pressure loads are applied, with the appropriate phase shift for each blade. In this first example, we used the standard Newmark scheme time-integration scheme with constant time step $\Delta t = 0.05s$.

The time history of the vertical displacement of the point C is plotted in Fig. 11. It is a sinusoidal curve that grows from the highest point (initial vertical position of C) to the lowest point. The peak-to-peak amplitude is equal to 2R. Thus, the entire load applied on each panel generates contributes to the rotational motion of the wind turbine blades. The first rotation period corresponds to start phase. It is lower when the wind increases, which gives a quicker start. After that the rotation periods are almost constant and equal to 4.9 s. Such a value is in perfect agreement with the rotor speed, imposed for panel method computation. This provides validation of the proposed panel method approach for simple wind load simulation of this kind.

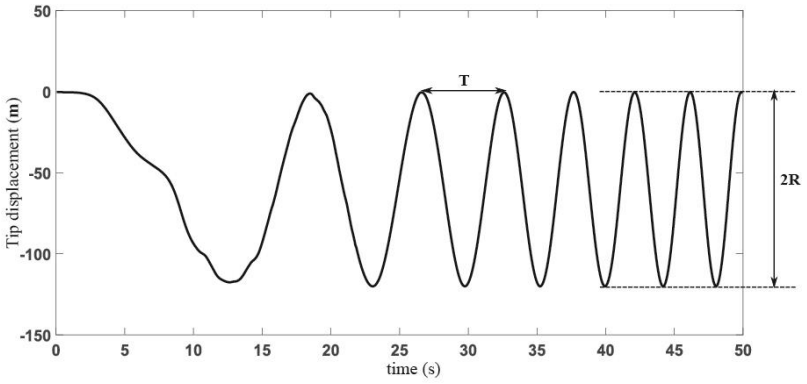

Fig. 11 Tip displacement in y-direction as function of time

As expected, the blade mostly displaces in the flap-wise direction, although some edgewise deflection is also present. Time histories of the flap-wise and edge-wise displacements at point C are shown in Fig. 12. The maximum flap-wise tip deflection reaches nearly 15 *m*, which is significant and can affect the stability of the wind turbine structure. We also note that the edge-wise deflection reaches its peak when it passes through its lowest vertical position (indicated in Fig. 4 as position 2). This finding is also consistent with the full-scale FSI results reported in (Bazilevs *et al.* 2011).

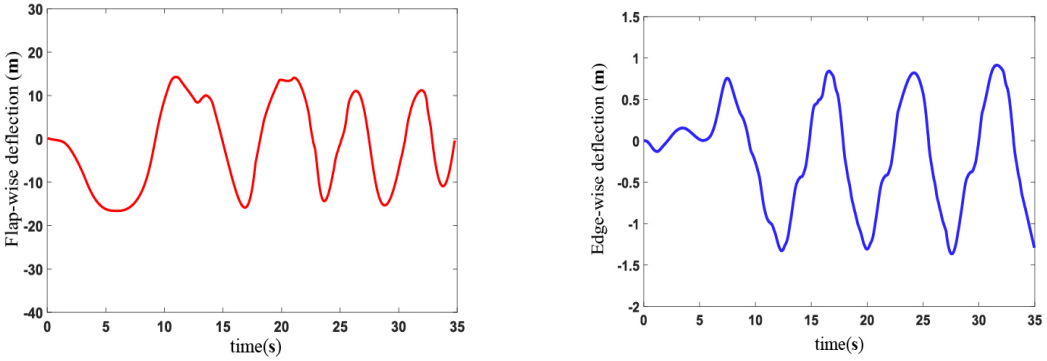

(a) Flap-wise deflection (b) Edge-wise deflection

Fig. 12 Time histories of in-plane and out-plane deflections in point C

In addition, the results of computation obtained by using proposed 3D solid elements are compared with those obtained by a standard solid element based on mixed formulation (Ibrahimbegovic 2009). In Fig. 13, time histories of displacement components in y-direction and z-direction are given for both configurations (point C). The computed results for rotation motion show a good agreement between the two formulations. We note that the bending vibrations in z-direction obtained by our 3D solid elements are greater than those obtained by the mixed element. This difference is primarily attributed to the use of incompatible modes, which allow increased accuracy in predicting the bending dominated motion in the case of low order solid elements.

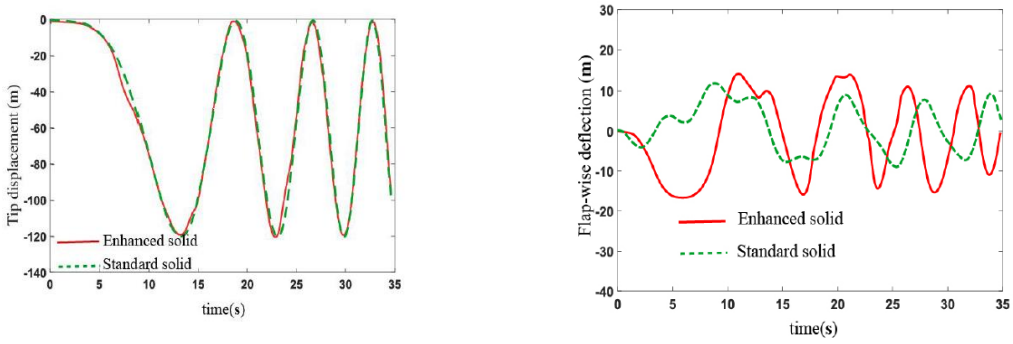

(a) Tip displacement (b) Flap-wise deflection

Fig. 13 Comparison between Enhanced and standard solid elements

4.2 Validation of the proposed conserving/decaying time-stepping schemes

In order to illustrate the proposed scheme capability to either conserve or decay energy, if desired to avoid instability induced by unresolved high frequencies, we further consider two long-term simulations.

First keeping the same model, computations are carried out by using the proposed conserving/decaying time-stepping schemes, and the results are compared against the corresponding ones obtained by using the Newmark scheme. The time step is $\Delta t = 0.05$ s. In Fig. 14, we present the high oscillations in the third component of the velocity of the housing obtained by the Newmark scheme against a smooth velocity response produced the proposed time-steeping scheme.

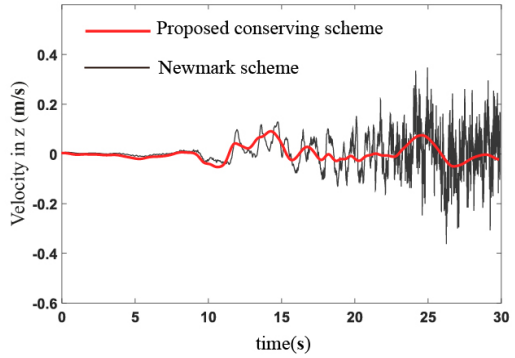

Fig. 14 Housing velocity in z-direction as function of time

Moreover, the computation using the Newmark scheme can no longer converge for time exceeding T = 50 s. However, the energy-conserving scheme ensures the convergence over long time interval (see Fig. 15), since that the accumulation of round-offs errors remains small by forcing the energy conservation at each time step. Furthermore, the energy-conserving ensures the scheme stability in long-term computations.

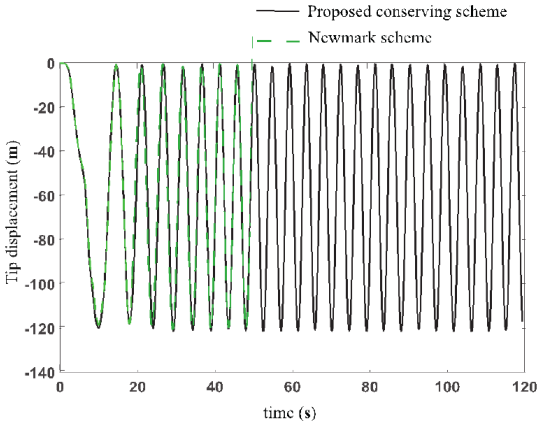

Fig. 15 Time history of tip displacement in y-direction: Long term simulation

In addition to the disturbed pressure obtained by panel method, the blades are subjected to perturbation-type forces in z-direction. These forces, applied over all blade surface, have a sinusoidal time variation with ω_p = 20 *rad*/s. The forces magnitude is equal to 8.10^2 *N*. The parameters of the perturbation-type load are chosen in order to trigger high mode bending vibrations.

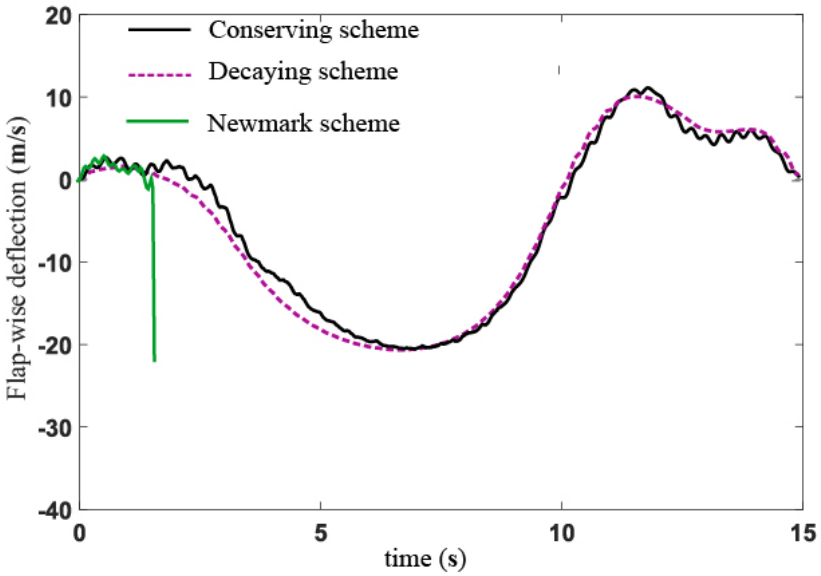

Fig. 16 Time history of flap-wise deflection: Time-stepping schemes

Time history of flap-wise deflection, plotted in Fig. 16, shows vibrations in z-direction obtained by superposition of resulting low and high frequency modes. The classical Newmark scheme is unable to provide any computational response, since the energy residual approaches infinity from the first steps. This confirms that the Newmark scheme is no longer appropriate and exhibits instabilities due to the presence of high frequency modes. However, for the energy-conserving schema, the residual remains sufficiently small to ensure the numerical stability. Therefore, it can be said that the proposed scheme overcomes the difficulties that occur in the presence of high frequency modes.

The numerical dissipation can be introduced with the energy-decaying scheme using $\boldsymbol{\eta_1 = \eta_2 = 0.1}$, which removes the high frequency noise and produces a smoother motion given in Fig. 16. The decaying-energy scheme serves as a filter that avoids the undesirable effect of high frequency contribution in numerical computation.

A similar tendency is observed in the time history of acceleration of the housing (nacelle) in z-direction, shown in Fig. 17. The acceleration computed by the Newmark scheme starts increasing quickly reaching unrealistic values. The energy-conserving scheme can keep the computation stable even in the presence of high frequency vibrations, but cannot eliminate them. However, the energy-decaying scheme seems fully capable to remove these high frequency vibrations, which often cannot be resolved without excessively fine mesh.

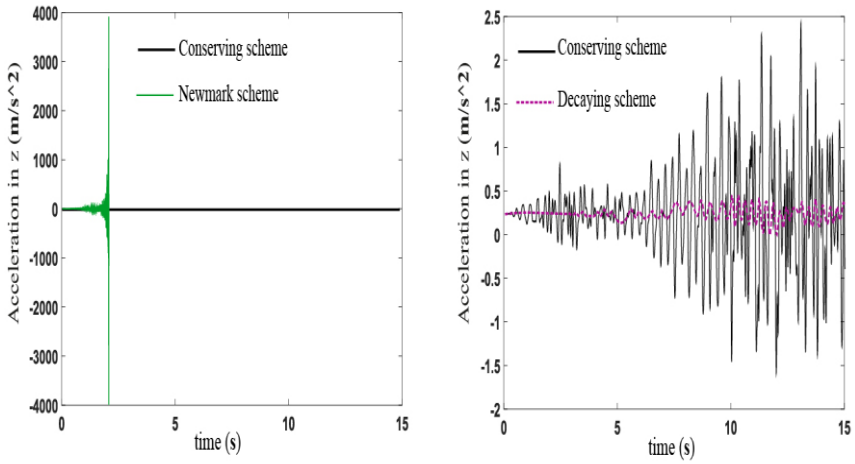

Fig. 17 Time history of acceleration in z-direction: time-stepping schemes

To conclude, the main advantage of the proposed time-stepping scheme is to provide wind turbines computational models, which are efficient in long-term simulation, even for extreme load conditions.

5. Conclusions

In this paper we have presented comprehensive yet efficient computational procedures for full-scale simulations of wind turbines. The procedure is targeting preliminary design parametric studies, and offers much needed efficiency by separating aerodynamics and structural mechanics computations. One of the key ingredients is in reliable wind loads prediction, cast in terms of follower pressure, which is here developed and thoroughly validated. This model is based upon the wind speed variation and the 3D panel method. For structural computation, we proposed a finite element model of wind turbine based upon 3D solid element with rotational degrees of freedom and incompatible modes. In fact, the wind turbine overall large motion is dominated by rotation about the rotor axis. To capture this, we found it advantageous to introduce the rotation tensor in the variational formulation in order to obtain an intrinsic representation of the blades rotation.

During long-term operation, wind turbines are subject to high frequency oscillations caused by the bending and torsional motion of the blades. The latter are extremely difficult to solve with reasonably refined mesh and standard implicit time-stepping schemes. Then, in this paper, we proposed time-stepping schemes that can ensure either energy-conserving or energy-decaying. We show that such schemes are needed in dynamic analysis of wind turbine models to improve the long-term numerical stability and avoid the undesirable effects of unresolved high frequencies.

Acknowledgments

This work was supported by French Ministry of Higher Education and Research, as well as the

funding by EU for Chair of Mechanics PICARDIE and by Institut Universitaire de France for IUF-Membre-Senior. This support is gratefully acknowledged. The authors would also like to thank the colleagues who wrote and helped us install Panel Method code, Professors William Devenport (Virginia Polytechnic) and Emmanual Lefrançois (UTC).

References

Ahlstrm, A. (2006), "Influence of wind turbine flexibility on loads and power production", *Wind Energy*, **9**, 237-249.

Boujelben, A. and Ibrahimbegovic, A. (2016), "Finite-strain three-dimensional solids with rotational degrees of freedom: Non-linear statics and dynamics", *Adv. Model. Simul. Eng. Sci.*, **4**, 646-654.

Spera, A.D. (1998), *Wind Turbine Technology, Fundamental Concepts in Wind Turbine Engineering*, ASME Press, New York, U.S.A.

Ibrahimbegovic, A. (1995), "On finite element implementation of geometrically nonlinear Reissners beam theory: Three-dimensional curved beam elements", *Comput. Meth. Appl. Mech. Eng.*, **122**, 11-26.

Ibrahimbegovic, A. (1997), "On the choice of finite rotation parameters", *J. Numer. Meth. Eng.*, **149**, 4971.

Ibrahimbegovic, A. (2009), *Nonlinear Solid Mechanics: Theoretical Formulations and Finite Element Solution Methods*, Springer Science and Business Media.

Ibrahimbegovic, A. and Mamouri, S. (2002), "Energy conserving/decaying implicit time-stepping scheme for nonlinear dynamics of three-dimensional beams undergoing finite rotations.", *Comput. Struct.*, **70**, 1-20.

Ibrahimbegovic, A., Kassiotis, C. and Niekamp, R. (2016), "Fluid-structure interaction problems solution by operator split methods and efficient software development by code-coupling", *Coupled Syst. Mech.*, **5**, 145-156.

Sanderse, B., Van Der Pijl, S.P. and Koren, B. (2011), "Review of computational fluid dynamics for wind turbine wake aerodynamics", *Wind Energy*, **14**, 799-819.

Webb, C. (2012), *Wind Turbine Blades Push Size Limits*, Renewable Energy World, July.

Hau, E. (2006), *Wind Turbines: Fundamentals, Technologies, Application, Economics*, 2nd Edition, Springer.

Lefrançois, E. (2017), "How an added mass matrix estimation may dramatically improve FSI calculations for moving foils", *Appl. Math. Model.*, **51**, 655-668.

Wilson, E.L. and Ibrahimbegovic, A. (1990), "Use of incompatible displacement modes for the calculation of element stiffnesses or stresses", *Fin. Elem. Analy. Des.*, **7**, 229-241.

European Commission (2017), *Renewable Energy Progress Report*, Brussels, February.

Cottet, G.H. and Koumoutsakos, P.D. (2000), *Vortex Methods: Theory and Practice*, Cambridge University Press, New York, U.S.A.

Imamovic, I., Ibrahimbegovic, A., Knopf-Lenoir, C. and Mesic, E. (2015), "Plasticity-damage model parameters identification for structural connections", *Coupled Syst. Mech.*, **4**, 337-364.

Simo, J.C. and Vu-Quoc, L. (1986), "A three-dimensional finite strain rod model. Part II: Geometric and computational aspects", *Comput. Meth. Appl. Mech. Eng.*, **58**, 79-116.

Simo, J.C., Taylor, R.L. and Wiggers, P. (1991), "A note on finite element implementation of pressure boundary loading", *Appl. Numer. Meth.*, **7**, 513-525.

Anderson, J.D. and Wendt, J. (1995), *Computational Fluid Dynamics*, McGraw-Hill, New York, U.S.A.

Jonkman, J., Butterfield, S., Musial, W. and Scott, G. (2005), *Definition of a 5-MW Reference Wind Turbine for Offshore System Development*, Technical Report NREL/TP-500-38060, National Renewable Energy Laboratory, Golden, CO.

Katz, J. and Plotkin, A. (1991), *Low-Speed Aerodynamics. From Wing Theory to Panel Methods*, McGraw Hill, New York, U.S.A.

Jonkman, J.M. and Matha, D. (2011), "Dynamics of offshore floating wind turbines analysis of three

concepts", *Wind Energy*, **14**, 557-569.
Rocca, J., Ibrahimbegovic, A. and Limnios, N. (2017), "Stochastic averaging for long-term response of dynamic systems", UTC Report, 1-15.
Spring, K.V. (1986), "Euler parameters and the use of quaternion algebra in the manipulation of finite rotations", *Mech. Mach. Theor.*, **21**, 365-373.
Biot, M.A. (1965), *Mechanics of Incremental Deformations*, John Wiley, London, U.K.
Hansena, M.O.L., Srensena, J.N., Voutsinasb, S., Srensenc, N. and Madsenc, H.A. (2006), "State of the art in wind turbine aerodynamics and aero elasticity", *Progr. Aerosp. Sci.*, **42**, 285-330.
Zienkiewicz, O.C. and Taylor, R.L. (1989), *The Finite Element Method: Basic Formulation and Linear Problems*, Vol. I, McGraw-Hill, Maidenhead, U.K.
Thresher, R.W., Wright, A.D. and Hershberg, E.L. (1986), "A computer analysis of wind turbine blade dynamic loads", *ASME J. Sol. Energy Eng.*, **108**, 17-25.
Breton, S.P. and Moe, G. (2009), "Status, plans and technologies for offshore wind turbines in Europe and North America", *Renew. Energy*, **34**, 3-27.
Law, S.P. and Gregorek, G.M. (1987), *Wind Tunnel Evaluation of a Truncated NACA 64-621 Airfoil for Wind Turbine Applications*, Technical Report, Ohio State University, Columbus, OH, U.S.A.
Hsu, S.A., Meindl, E.A. and Gilhousen, D.B. (1994), "Determining the Power-law wind-profile exponent under near-neutral stability conditions at sea", *J. Appl. Meteorol. Climatol.*, **33**, 757-765.
Siemens AG, Energy Sector (2011), *Siemens Wind Turbine SWT-2.3-108: The New Productivity Benchmark*, Technical Report.
Do, X.N., Ibrahimbegovic, A. and Brancherie, D. (2015a), "Combined hardening and localized failure with softening plasticity in dynamics", *Coupled Syst. Mech.*, **4**, 115-136.
Do, X.N., Ibrahimbegovic, A. and Brancherie, D. (2015b), "Localized failure in damage dynamics", *Coupled Syst. Mech.*, **4**, 211-235.
Bazilevs, Y. and Hsu, M.C. (2012), "ALE-VMS and ST-VMS methods for computer modeling of wind turbine rotor aerodynamics and fluid-structure interaction", *Math. Model. Meth. Appl. Sci.*, **22**, 1-62.
Bazilevs, Y., Hsu, M.C., Kiendl, J., Wchner, R. and Bletzinger, K.U. (2011), "3D simulation of wind turbine rotors at full scale. Part II: Fluid structure interaction modeling with composite blades", *J. Numer. Meth. Flu.*, **65**, 236-253.

AI